AMERICAN SOCIETY FOR MICROBIOLOGY | mSystems®

RESEARCH ARTICLE

# A Dual-Functional Orphan Response Regulator Negatively Controls the Differential Transcription of Duplicate *groELs* and Plays a Global Regulatory Role in *Myxococcus*

**Li Zhuo,[a] Tian-yu Wan,[a] Zhuo Pan,[a] Jia-ning Wang,[a] Duo-hong Sheng,[a] Yue-zhong Li[a]**

[a]State Key Laboratory of Microbial Technology, Institute of Microbial Technology, Shandong University, Qingdao, People's Republic of China

**ABSTRACT** Differential transcription of functionally divergent duplicate genes is critical for bacterial cells to properly and competitively function in the environment, but the transcriptional regulation mechanisms remain in mystery. *Myxococcus xanthus* DK1622 possesses two duplicate *groEL*s with divergent functions. Here, we report that *MXAN_4468*, an orphan gene located upstream of *groEL2*, encodes a response regulator (RR) and is responsible for the differential expression regulation of duplicate *groEL*s. This RR protein realizes its negative regulatory role via a novel dual-mode functioning manner: binding to the transcription repressor HrcA to enhance its transcriptional inhibition of duplicate *groEL*s and binding to the 3′ end of the *MXAN_4468* sequence to specifically decrease the transcription of the following *groEL2*. Phosphorylation at the conserved 61$^{st}$ aspartic acid is required to trigger the regulatory functions of MXAN_4468. Pull-down experiment and mutation demonstrated that two noncognate CheA proteins, respectively belonging to the Che8 and Che7 chemosensory pathways, are involved in the protein phosphorylation. A transcriptome analysis, as well as the pull-down experiment, suggested that MXAN_4468 plays a global negative regulatory role in *M. xanthus*. This study elucidates, for the first time, the regulatory mechanism of differential transcription of bacterial duplicate *groEL*s and suggests a global regulatory role of a dual-functional orphan RR.

**IMPORTANCE** Multiply copied *groEL*s require precise regulation of transcriptions for their divergent cellular functions. Here, we reported that an orphan response regulator (RR) tunes the transcriptional discrepancy of the duplicate *groEL*s in *Myxococcus xanthus* DK1622 in a dual-functional mode. This RR protein has a conserved phosphorylation site, and the phosphorylation is required for the regulatory functions. Transcriptomic analysis, as well as a pull-down experiment, suggests that the RR plays a global regulatory role in *M. xanthus*. This study highlights that the dual-functional orphan RR might be involved in conducting the transcriptional symphony to stabilize the complex biological functions in cells.

**KEYWORDS** two-component system, orphan response regulator, duplicate *groEL*s, differential transcription, *Myxococcus*

Two-component systems (TCSs) serve as the basic stimulus-response coupling mechanism allowing bacterial cells to sense and respond to diverse changes in environment (1, 2). Typically, a TCS consists of a histidine kinase (HK) and a cognate response regulator (RR). HK undergoes an ATP-dependent autophosphorylation of a conserved histidine (His) residue upon stimulation, creating a high-energy phosphoryl group that is subsequently transferred to the aspartate (Asp) residue of the downstream RR. Then the phosphorylated RR activates or represses transcription of target genes (1, 3). Although paired HK and RR may function efficiently, orphan RR is universal in bacteria in a broad range of numbers and ratios For instance, 5 of the 32 RRs in

**Editor** Rafael Silva-Rocha, FMRP-USP



Address correspondence to Yue-zhong Li, lilab@sdu.edu.cn.

The authors declare no conflict of interest.

**Received** 19 August 2021
**Accepted** 4 March 2022
**Published** 30 March 2022

*Escherichia coli* are orphan (4), 2 of the 20 RRs in *Streptococcus sobrinus* are orphan (5), and 2 of the 16 RRs in *Acinetobacter baumannii* are orphan (6). In comparison, *Myxococcus xanthus* possesses a total of 119 RRs, and more than 50% of them are orphan (7). During the past decade, functions of orphan RRs have been investigated in some bacteria, for example, in *Streptomyces* (8). However, little is known about the regulatory mechanisms of orphan RRs.

GroEL is an important molecular chaperone that belongs to the Hsp60 family of heat shock proteins, and it is involved in diverse biological functions in bacterial cells by participating in folding, maturation, and transport of many proteins under normal growth or heat shock conditions (9, 10). Most bacteria have a single copy of *groEL*, but the presence of two or more copies has been identified in 19.5% of the sequenced bacterial genomes (11). Duplicate *groEL*s are strictly transcribed at different levels, to fit their divergent cellular functions. For example, *M. xanthus* DK1622 has duplicate *groEL*s: *groEL1* plays an essential role in development and sporulation, while *groEL2* is required for cell predation and biosynthesis of the secondary metabolite myxovirescin (12–14). The transcriptional levels of these two *groEL*s are significantly different: the transcriptional level of *groEL1* is normally four times that of *groEL2*, and the transcriptional level of single *groES*, which is required for the functions of duplicate *groEL*s, is almost the sum of the *groEL1* and *groEL2* transcriptional levels (11). We previously reported that the global positive regulator $\sigma^{32}$ and the local negative regulator HrcA are involved in the transcriptional regulation; these two regulators respectively target the $-10/-35$ region and the CIRCE element, which are separate in the promoter of *groEL1* but overlapped in that of *groEL2* (15). However, the regulation of $\sigma^{32}$ and HrcA does not explain the strictly differential transcription of duplicate *groEL*s.

In *M. xanthus* DK1622, the *groEL1* and *groEL2* genes have distinct compositions and locations on the genome; *groEL1* (*MXAN_4895*) is located in a *groESL* operon, while *groEL2* (*MXAN_4467*) has no neighboring *groES* and is downstream of *MXAN_4468*, which encodes an orphan RR. In this study, we found that *MXAN_4468* deletion eliminated the negative transcriptional control of both *groEL*s and increased the expression of *groEL2* to almost the same level as that of *groEL1*. The RR has a conserved phosphorylation site, and phosphorylation of this Asp residue is required to trigger the RR regulatory functions. Pull-down assay and mutation indicated that two CheA proteins might be the noncognate HKs of this orphan RR. We determined that the regulator plays a central role for differential expression of duplicate *groEL*s in a dual-functioning mode: it enhances the ability of HrcA to bind to the CIRCE sequences to regulate the transcription of *groEL1* and *groEL2*, and it binds to the 3′ end of its own gene sequence to specifically negatively control the transcription of the downstream *groEL2* gene. A network analysis based on the transcriptome data, as well as the pull-down experiment, suggested that the RR gene plays a global negative regulatory role and primarily affects the transcription of stress regulatory proteins. This study highlights that this orphan RR in *M. xanthus* cells negatively regulates the transcription of duplicate *groEL*s and is involved in the control of complex biological functions.

## RESULTS

**The RR gene upstream of *groEL2* is a negative regulator of the transcription of duplicate *groEL*s in *Myxococcus xanthus*.** *M. xanthus* DK1622 has two *groEL*s and one *groES*; *groEL1* forms a complete operon with the single *groES*, and *groEL2* exists alone. *MXAN_4468* lies upstream of *groEL2* and is annotated by NCBI to encode a response regulator (RR) belonging to the cdd388505 protein family. *MXAN_4468* is an orphan RR. We found that the RR gene is located adjacent to *groEL2*, upstream and/or downstream, in a phylogenetically specific manner in different myxobacteria but does not occur adjacent to *groEL1* (Fig. 1A; see also Table S1 in the supplemental material). Based on the sequenced myxobacterial genomes, the *MXAN_4468* homologues locate upstream of *groEL2* in the same direction in *Myxococcus* genomes, downstream of *groEL2* in the opposite direction in *Anaeromyxobacter* genomes, and upstream and downstream of *groEL2* in the genomes of the genera *Corallococcus*, *Stigmatella*, and *Cystobacter*. However, there is no RR gene

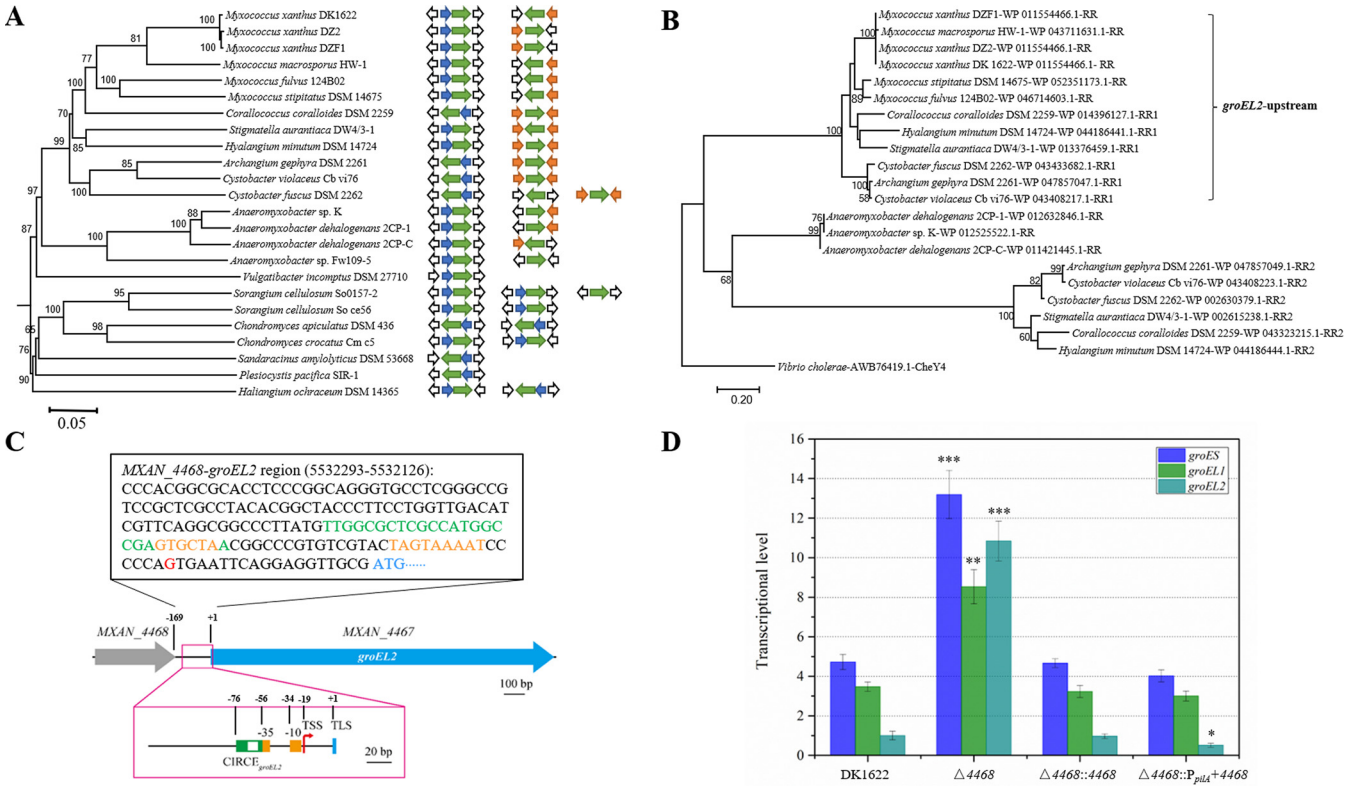


**FIG 1** The RR genes in myxobacteria. (A) The composition and organization of the *groEL*, *groES*, and RR genes in the 24 sequenced myxobacterial genomes. The green, blue, and orange arrows show the transcription direction of the *groEL*, *groES*, and RR genes, respectively. (B) Evolutionary relationship analysis of myxobacterial RR neighboring *groEL*s. *Vibrio cholerae* chemotaxis-associated protein CheY4 was used as the outroot. (C) Representation of the region of *groEL2* and *MXAN_4468* in *M. xanthus* DK1622. The bar in the panel equals a 20-bp distance. (D) qPCR analysis of the transcriptional levels of *groES* and *groEL*s in *MXAN_4468* knockout, complementation, and overexpression mutants and the wild-type strain DK1622 after 24 h of incubation. The transcriptional level of *groEL2* in DK1622 was set to 1. For statistical analysis, "***," "**," and "*" indicate *P* values of <0.001, <0.01, and <0.05, respectively.

adjacent to *groEL2* in the genomes of the *Sorangineae* suborder (Fig. 1A). The RR proteins encoded by the upstream genes are highly conserved, the second RR proteins encoded by the downstream RR genes are closely grouped in a separate branch, and the single downstream RRs in the *Anaeromyxobacter* genomes form the third branch (Fig. 1B). These phylogenetically conserved RR genes might have similar cellular functions critical for myxobacteria.

The *MXAN_4468* and *groEL2* genes are separated by a 169-bp sequence, and the two genes were confirmed to be transcribed by their own promoters (Fig. 1C and Fig. S1A). This interval sequence contains the core promoter region of *groEL2*, which includes a CIRCE sequence for binding the negative regulator HrcA (15). We found that deletion of the RR gene greatly increased the transcriptional levels of *groES*, *groEL1*, and *groEL2* in DK1622 (Fig. 1D; *t* test, *groES* and *groEL2*, *P* value $< 0.001$; *groEL1*, *P* value $< 0.01$). The increases in the transcriptional levels of *groES* and *groEL*s were completely abolished by the *in situ* complementation of *MXAN_4468*. However, *in situ* overexpression of *MXAN_4468* had no effect on the transcription of *groES* and *groEL1* but significantly decreased *groEL2* expression (Fig. 1D; *t* test, *P* value $< 0.05$). The RR gene deletion, complementation, and overexpression were confirmed by quantitative PCR (qPCR) analysis (Fig. S1B). The above-described results indicate that *MXAN_4468* is a strong negative regulator of the expression of *groES* and *groEL*s and has an additional inhibitory effect specifically on *groEL2*. The transcriptional curves of *groES* and *groEL*s in the *MXAN_4468* knockout strain indicated that compared with wild-type DK1622, the negative regulation of *groES* and *groEL*s by the *MXAN_4468* gene occurred mainly in the exponential growth phase, when the chaperonin genes were expressed under either the normal temperature condition (30°C) or after heat shock at 42°C for 1 h (Fig. S1C). Notably, according to the transcriptome data, the

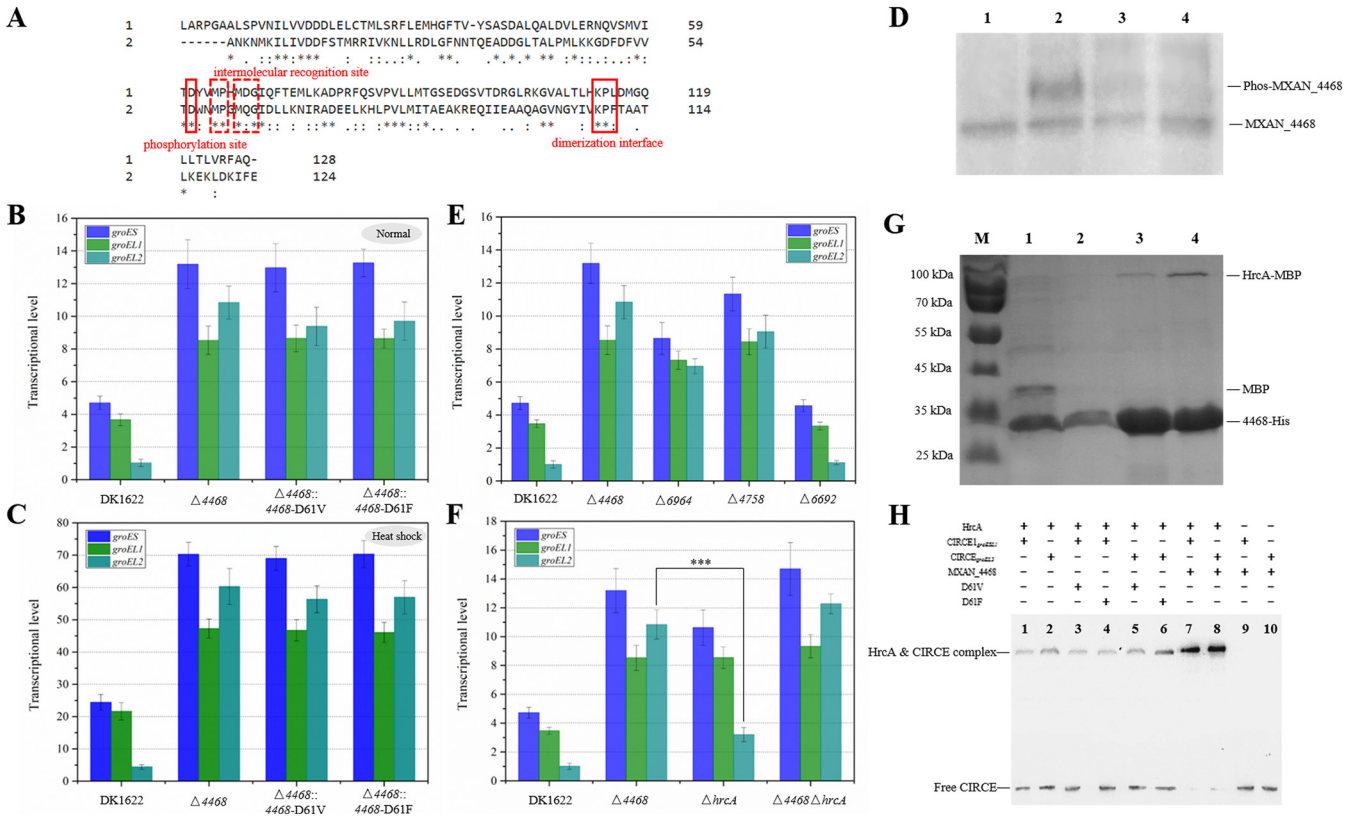


**FIG 2** Phosphorylated MXAN_4468 binds to HrcA to inhibit the *groESL* transcription. (A) Bi-sequence alignment analysis of *M. xanthus* MXAN_4468 protein and *Vibrio cholerae* chemotaxis-associated protein CheY4. Alignments 1 and 2 are the amino acid sequences of *M. xanthus* MXAN_4468 and *Vibrio cholerae* CheY4, respectively. The red solid lines indicate phosphorylation sites and the dimerization interface, and the red dashed lines represent intermolecular recognition sites. (B and C) The transcriptional levels of *groES*, *groEL1*, and *groEL2* in *M. xanthus* DK1622 and *MXAN_4468* mutants grown in CTT medium at a normal temperature (B) and at heat shock for 1 h more (C). The transcriptional level of *groEL2* in the wild-type DK1622 under the normal condition was set to 1. (D) Phos-tag PAGE analysis of MXAN_4468 mutants. Lane 1, purified 4468-His protein cloned in *E. coli*; lane 2, Δ*4468*::*4468*-His wild-type strain; lane 3, Δ*4468*::*4468*-D61V-His mutant; lane 4, Δ*4468*::*4468*-D61F-His mutant. For all of the assay, no additional HK proteins were added. (E) qPCR analysis of the transcriptional levels of *groES* and *groEL*s in the *MXAN_4468* knockout mutant, the two *cheA* deletion mutants, the *MXAN_6692* knockout mutant, and wild-type strain DK1622 after 24 h of incubation. (F) qPCR analysis of the transcriptional levels of *groES* and *groEL*s in *MXAN_4468* and *hrcA* knockout mutants and the *MXAN_4468* and *hrcA* double-deletion mutant. For statistical analysis, "****" means *P* value of <0.001. The transcriptional level of *groEL2* in the wild-type DK1622 was set to 1 (E and F). (G) Pull-down analysis of MXAN_4468 and HrcA detected by SDS-PAGE. M, marker: PageRuler$^{TM}$ prestained protein ladder. Lane 1, MBP protein plus MXAN_4468-His protein penetrating liquid; lane 2, MBP protein plus MXAN_4468-His 250 mM imidazole elution product; lane 3, HrcA-MBP plus MXAN_4468-His penetrating liquid; lane 4, HrcA-MBP plus MXAN_4468-His 250 mM imidazole-elution product. (H) Effects of the addition of MXAN_4468 and MXAN_4468 mutant proteins (D61V and D61F) on the interaction between HrcA and CIRCE (presented by native PAGE). The components added in each lane are labeled at the top.

transcription of *MXAN_4468* was significantly changed at 24 h and 36 h under the normal and heat shock conditions (Fig. S1D).

**The orphan MXAN_4468 is phosphorylated by two noncognate CheAs belonging to the Che8 and Che7 chemosensory pathways.** MXAN_4468 is a single-domain RR, which is represented by the chemotaxis-associated protein CheY (16). This protein has the highest sequence identity with CheY4 of *Vibrio cholerae* (42.48%), and the two proteins are also highly similar in structure based on the modeling analysis (Fig. S2A). CheY4 is involved in chemotaxis-related motility to control the direction of flagellar movement (17, 18). Active CheY4 is a phosphorylated protein, and the phosphorylated amino acid is located in the domain that receives signals transmitted from the upstream component (19). Based on the amino acid sequence alignment with CheY4, MXAN_4468 may contain a similar phosphorylation site at the 61$^{st}$ aspartic acid (Fig. 2A). Notably, *M. xanthus* DK1622 has 20 single-domain RR homologues belonging to the cdd388505 protein family (Table S1), and some of them have been annotated in different chemosensory pathways (20, 21). These 20 RR homologues in *M. xanthus* DK1622 (Fig. S2B), as well as the 21 *groEL2*-adjacent RRs in different myxobacterial genomes (Fig. S2C), were all conserved at the 61$^{st}$ aspartic acid.

To explore the phosphorylation and its functional effects, we mutated the *MXAN_4468* gene by altering the 61st aspartic acid to valine and phenylalanine in the DK1622 genome according to references 22 and 23), producing the Δ*4468*::*4468*-D61V and Δ*4468*::*4468*-D61F mutant strains, respectively. This amino acid swapping led to almost the same transcriptional levels of *groES* and *groEL*s as those in the *MXAN_4468* knockout mutant under either normal temperature or heat shock conditions (Fig. 2B and C). To facilitate the phosphorylation check, we further linked a 6×His-encoding sequence to the C terminus of *MXAN_4468* in the wild-type DK1622 and the two mutants. The Phos-tag PAGE analysis showed that only purified MXAN_4468 protein with no addition of HK was not phosphorylated (Fig. 2D, lane 1). However, the MXAN_4468 protein in the supernatant of DK1622, which contains HKs, was phosphorylated (lane 2), but both the the 61st mutant proteins in mutant strains, which also contain HKs, were not (lanes 3 and 4) (Fig. 2D). The results indicate that the 61st aspartic acid is the phosphorylation site of MXAN_4468, and phosphorylation of this amino acid is essential for MXAN_4468 to regulate the transcription of *groES* and *groEL*s.

We performed a pull-down assay of the MXAN_4468 wild-type protein, as well as the D61V and D61F mutant proteins, with the supernatant of disrupted DK1622 cells to screen its potential interacting proteins. The expression and purification of these proteins are shown in Fig. S2D. We noticed that the proteins specifically bound by MBP-MXAN_4468 included two CheA proteins, MXAN_4758 and MXAN_6964, which, however, were not among the binding proteins of the two MXAN_4468 mutants (Table S2). CheA proteins are HKs that are responsible for transferring the phosphoryl group to the RRs in the corresponding TCSs (24, 25). MXAN_4468 is an orphan RR, and the two CheA proteins may be the noncognate HKs for the phosphorylation of MXAN_4468. Interestingly, the *MXAN_4758* and *MXAN_6964* genes belong to the Che8 and Che7 chemosensory pathways, respectively (21). The Che7 system has been reported to be associated with a HEAT repeat domain-containing protein and required for the appropriate coupling of aggregation and sporulation, while the functions of the Che8 system have not yet been identified (21, 26). We knocked out each of the two *cheA* genes from the DK1622 strain. The two deletions led to similar transcriptional levels of *groESL* genes as that resulting from *MXAN_4468* deletion (Fig. 2E). Comparably, the *MXAN_4758* (*cheA8*) deletion mutant had a closer transcriptional level of *groESL* to that of the *MXAN_4468* deletion mutant than the *MXAN_6964* (*cheA7*) deletion mutant. Notably, in the eight chemosensory pathways (21), while five CheA proteins are hybrid HKs (CheA-RR fusion protein) responsible for autophosphorylation, three are typical HKs (single-domain CheA), including the above-mentioned two CheAs and MXAN_6692. The latter is in the Dif chemosensory pathway and was not bound by MXAN_4468 in the pull-down assay. We similarly deleted the *MXAN_6692* gene, which, however, did not change the transcription of *groESL*s (Fig. 2E). The above-described results strongly suggest that *MXAN_4758* and *MXAN_6964* are both responsible for the phosphorylation of MXAN_4468 protein and that *MXAN_4758* is probably more important for this process.

**Phosphorylated MXAN_4468 binds to HrcA to inhibit *groESL* transcription.** HrcA (MXAN_6726) is a negative transcription regulator of duplicate *groEL*s (15). This protein was also pulled down by MXAN_4468 but was not by the two MXAN_4468 mutants. Compared to the Δ*hrcA* mutant, the Δ*4468* mutant showed almost unchanged *groES* and *groEL1* transcriptional levels, but its *groEL2* transcriptional level was approximately three times higher (*t* test, *groEL2*, $P$ value $< 0.001$). Further deletion of *hrcA* in the Δ*4468* mutant caused no more changes in the *groES* and *groEL*s transcriptional levels (Fig. 2F; *t* test, *groES*, $P$ value = 0.122; *groEL1*, $P$ value = 0.141; *groEL2*, $P$ value = 0.088). Thus, compared to the double deletion mutant of *MXAN_4468* and *hrcA*, only *hrcA* without *MXAN_4468* (Δ*4468*) had almost no regulatory effect on the transcription of *groES* and *groEL*s, only *MXAN_4468* without *hrcA* (Δ*hrcA*) negatively and specifically regulated the transcription of *groEL2*, and the presence of both *hrcA* and *MXAN_4468* (DK1622) led to negative regulation of the transcription of *groES* and *groEL*s. The results suggest that

MXAN_4468 not only cooperates with HrcA on the transcriptional regulation of *groES* and *groEL*s but also alone specifically inhibits the transcription of *groEL2*.

To investigate the binding ability between MXAN_4468 and HrcA, we constructed two recombinant expression vectors, *4468*-pET32a and *hrcA*-pMAL-c5x, and labeled the C termini of MXAN_4468 and HrcA with His and maltose binding protein (MBP) tags, respectively (the purification of HrcA protein is shown in Fig. S2E). *In vitro* pull-down experiments showed that although there existed some excess proteins in penetrating liquid (Fig. 2G, lane 3), 4468-His and HrcA-MBP were both absorbed on beads for His proteins in the elution of imidazole washing buffer (lane 4), while MBP, mixed with 4468-His, was not absorbed on beads (lane 2). This result further confirmed the presence of a binding interaction between the MXAN_4468 and HrcA proteins.

Through electrophoretic mobility shift assay (EMSA) and isothermal titration calorimetry (ITC) binding experiments, we previously proved that HrcA has the capacity to bind CIRCE1$_{groESL1}$ or CIRCE$_{groEL2}$ but no capacity to interact with CIRCE2$_{groESL1}$ in *M. xanthus* DK1622 (15). To investigate whether MXAN_4468 affected the binding reaction of HrcA and CIRCE, we added MXAN_4468 and its mutants of D61V and D61F to the reaction mixtures. As shown in Fig. 2H, HrcA alone formed a weak blocking band with CIRCE1$_{groESL1}$ or CIRCE$_{groEL2}$, and the addition of MXAN_4468, but not the MXAN_4468 mutants, significantly enhanced the brightness of the blocking band and completely weakened the brightness of DNA band (lanes 7 and 8); MXAN_4468 itself was unable to bind to the CIRCE elements (lanes 9 and 10). The weak binding ability of HrcA alone to CIRCE sequences suggests its regulatory effect on the transcription of *groES* and *groEL*s, which, however, is inconsistent with the phenotypic comparison results of the Δ*4468* and Δ*4468* Δ*hrcA* mutants (Fig. 2F). In *M. xanthus* DK1622, CIRCE1$_{groESL1}$ and CIRCE$_{groEL2}$ sequences overlap the transcription start site (TSS) and −35 regions of the promoters of *groEL1* and *groEL2*, respectively, and these regions are the binding targets of many essential factors for transcription, such as $\sigma^{32}$ and HrcA regulators (15). We suggest that the binding of MXAN_4468 to HrcA is necessary for the regulatory role of HrcA in the transcription of *groES* and *groEL*s, probably by enhancing the binding competition ability of HrcA to the CIRCE sequences.

**Phosphorylated MXAN_4468 binds to its own gene sequence to specifically inhibit the transcription of the downstream *groEL2*.** The interval sequence between *MXAN_4468* and *groEL2* is 169 bp long and contains the promoter region of *groEL2*. Because *MXAN_4468* deletion had an additional specific effect on the transcription of *groEL2*, we inferred that the deletion fragment of the Δ*4468* mutant probably contained a regulatory sequence to which MXAN_4468 binds to negatively and specifically regulate the transcription of *groEL2*. To investigate whether there is such a regulatory sequence, we further constructed four mutants at different positions to retain the 3′ end of *MXAN_4468* (Fig. 3A). Briefly, while the 3′-terminal regions were retained in the four partial mutants, the deleted regions were different: in KI68-1, only the 5′-terminal region of *MXAN_4468* was deleted; in KI68-2 and KI68-3, the deleted regions included the promoter region and different 5′-terminal regions (retaining the 61$^{st}$ phosphorylation site or not) of *MXAN_4468*; and in KI68-4, the deletion included the 3′ terminus of the upstream *MXAN_4469*, the promoter region, and a 5′-terminal region of *MXAN_4468*. We did not additionally express the *MXAN_4468* gene in other places of the genome. We found that the transcriptional levels of *groES* and *groEL1* in these four incomplete deletion mutants of *MXAN_4468* were the same as those in the complete deletion mutant, but the transcriptional level of *groEL2* was much lower (Fig. 3B) and was almost the same as that in the Δ*hrcA* mutant (refer to Fig. 2F). Compared to the double deletion mutant of *MXAN_4468* and *hrcA*, the existence of the 3′-end region of *MXAN_4468* and complete *hrcA* (KI68 mutants) had a more negative regulatory effect on the *groEL*2 transcription, similar to that in the mutant with *MXAN_4468* but not *hrcA* (Δ*hrcA*). In other words, the 3′-end region of *MXAN_4468* would be essential to maintain the lower expression of *groEL2*, regardless of the existence of *hrcA*. The results indicate that the 3′-end region of *MXAN_4468*, which was retained in the *MXAN_4468*-

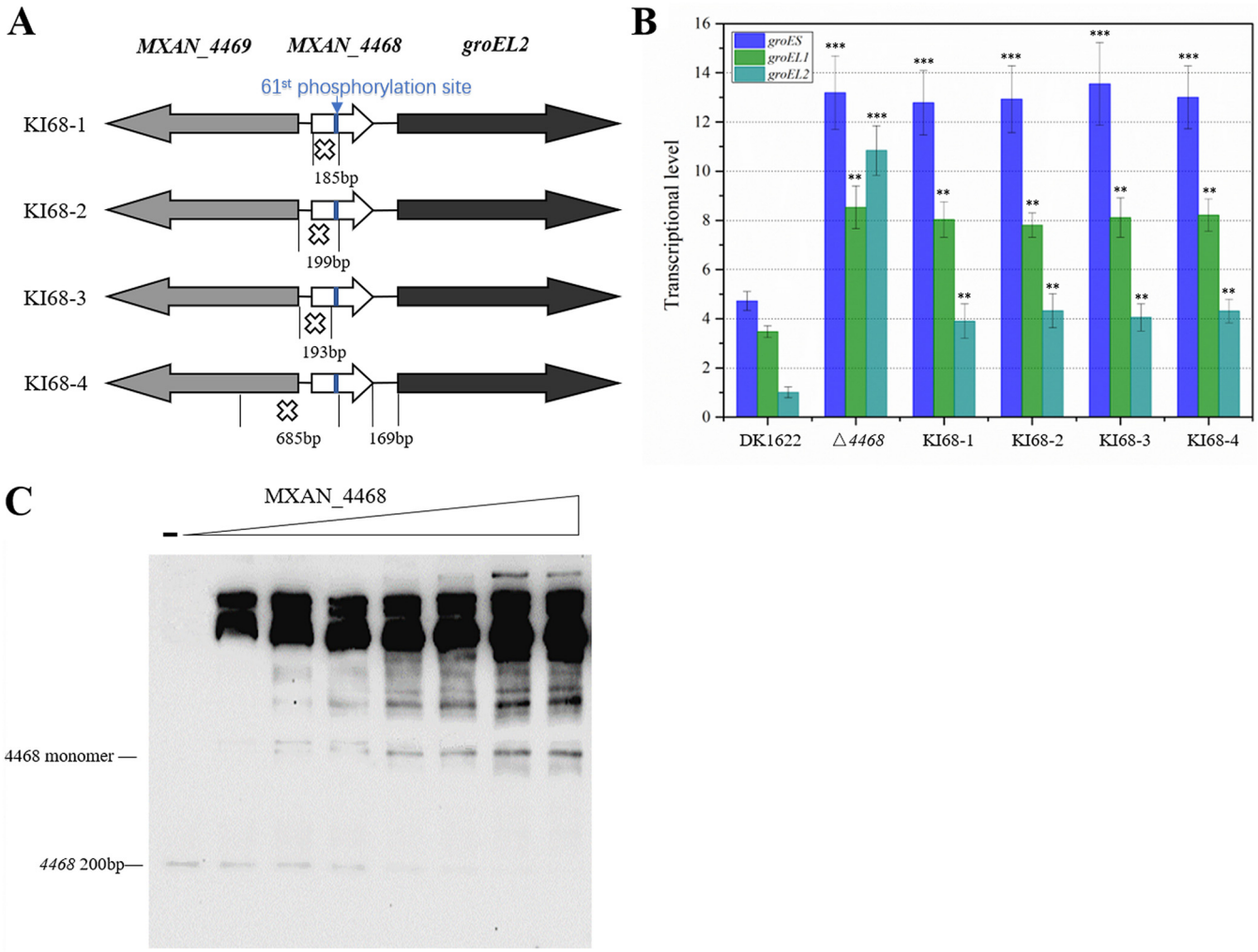


**FIG 3** The transcriptional relationship between *MXAN_4468* and its own coding region. (A) Representations of the *MXAN_4468* knockout mutants. (B) qPCR analysis of the transcriptional levels of *groES* and *groEL*s in *MXAN_4468* knockout mutants and the wild-type strain DK1622. The transcriptional level of *groEL2* in DK1622 was set to 1. For statistical analysis, "***" and "**" mean *P* values of $<0.001$ and $<0.01$, respectively. (C) Analysis of binding activity between the MXAN_4468 protein and the inner 200-bp 3′-end sequence of *MXAN_4468* using EMSA (presented by native PAGE). The monomers of the MXAN_4468 protein are marked in the diagram. Other protein bands with high concentrations were proven to be the polymers of MXAN_4468 (Fig. S3B to D).

incompletely deleted mutants, contains a sequence that is for the specific negative regulation of *groEL2* transcription.

To confirm this unusual regulatory mechanism, we performed an EMSA of the MXAN_4468 proteins with the upstream 370-bp sequence of *groEL2* (Fig. S3A) or the inner 200-bp 3′-end sequence of *MXAN_4468* (Fig. 3C). The results showed that there were obvious blocking bands between the MXAN_4468 protein and the two DNA sequences, and the brightness of the DNA-protein complexes was enhanced with an increase in the concentration of MXAN_4468 protein. These blocking bands were determined by mass spectrometry to be MXAN_4468 (Fig. S3B to D) and were presumed to be the monomeric and polymeric forms of MXAN_4468. The band intensity showed that the MXAN_4468 proteins preferred to bind to their own DNA sequence in polymeric forms. Besides MXAN_4468, there exist other 19 single-domain RR homologues in *M. xanthus* DK1622 (Table S1), which were probably able to bind to the 3′-end region of *MXAN_4468* to decrease the *groEL2* transcription. Compared to the *MXAN_4468* complete knockout mutant, the four incomplete deletion mutants (KI68 mutants) had lower *groEL2* transcription (Fig. 3B). In addition, the mutated MXAN_4468 proteins were observed in the Δ*4468*::*4468*-D61V and Δ*4468*::*4468*-D61F strains (Lanes 3 and 4 in Fig. 2D), i.e., the *MXAN_4468* gene was expressed and still maintained the 3′-end region,

but the two mutant strains exhibited almost the same *groES* and *groEL*s transcriptional levels as those exhibited by the Δ*4468* mutant, especially for *groEL2* transcription. Due to the distance advantage of the *MXAN_4468* gene, nonphosphorylated MXAN_4468 proteins could combine with the 3′-end region of *MXAN_4468*, thus preventing the binding of other MXAN_4468 homologues on the location. However, the interaction would not lead to negative regulation on the *groEL2* transcription because of nonphosphorylation of the mutated MXAN_4468 proteins. We conclude that the phosphorylated MXAN_4468 protein specifically inhibits the transcription of *groEL2* by binding to its own sequence, thus interfering with the binding of transcriptional factors to the promoter of the downstream *groEL2* gene.

**Global effects of *MXAN_4468* deletion in *M. xanthus* DK1622 cells.** Our abovementioned results demonstrated that the phosphorylated MXAN_4468 protein plays a critical role in regulation of the expression of *groES* and *groEL*s, leading to their differential transcriptional levels. GroEL is a type I chaperonin and an essential component in different bacterial species (27, 28). It is required for correct *in vivo* folding of more than 10% of the total proteins in *E. coli* (10). Our previous studies indicate that the protein clients of the *M. xanthus* GroELs, although consistent with those of the single *E. coli* GroEL in their secondary structural features, vary significantly in the substrate spectra, and GroEL1 and GroEL2 have their own exclusive protein clients in addition to the shared clients (13). Moreover, the proteins that were specifically pulled down by MXAN_4468 included not only the CheA and HrcA proteins but also some other regulatory proteins, such as an RNA polymerase sigma 70 factor (MXAN_7454), a transcriptional regulator (MXAN_1757), a sigma 54 transcriptional regulator (MXAN_0907), which are related to stress and transcriptional regulation (Table S2) (the energies for binding of these three proteins to MXAN_4468 were estimated by the JSmol website to be −28.47, −21.32, and −10.97, respectively). These results suggested that MXAN_4468 probably plays a global transcriptional regulator role, not only via the control of transcriptional levels of *groESL*s but also via other regulatory proteins. To explore potential global effects, we performed a transcriptome analysis on the *MXAN_4468* knockout strain and the wild-type strain DK1622 using cells grown for 24 h and 36 h under the normal temperature or heat shock condition. We BLAST searched the reads of transcriptome data against the reference genome of DK1622 using the Bowtie2 program (29) and found that the total mapped value of all samples exceeded 99% (Table S3), which indicates that the samples were not contaminated and that the transcriptome data were reliable.

We found that the transcriptomes of the Δ*MXAN_4468* strain and DK1622 had significant differences (Fig. S4; for details, see Data Set S1 [sheets 1 to 4]). Functional annotation of the differentially expressed genes in the cells grown for 24 h under the normal temperature condition indicated that the genes that were significantly upregulated by *MXAN_4468* deletion were mainly related to the two-component system and metabolism, while those that were significantly downregulated were mainly related to ribosomes and binding proteins (Fig. 4A). After heat shock, the most significantly upregulated genes were involved in the pathways of metabolism and phosphotransferase system, and the most significantly downregulated genes were related to partial amino acid degradation and oxidative phosphorylation. Under the 36-h normal temperature and heat shock conditions, the significantly upregulated genes were related to amino acid and RNA degradation, and the significantly downregulated genes were related to metabolism and amino acid biosynthesis.

To highlight the transcriptional impacts of the *MXAN_4468* deletion, we performed a network analysis of the top 200 differentially expressed genes in all transcriptome samples. These top 200 genes were classified into four classes according to their annotation: stress regulatory proteins (40), metabolites (66), ribosomal proteins (39), and unknown proteins (55) (Data Set S1 [sheets 5 to 8]). Notably, the genes encoding stress regulatory proteins were mostly upregulated (36 of 40; the gene names in white with a purple background in Fig. 4B), while the genes encoding metabolites and ribosomal proteins were either upregulated or downregulated (colored in purple or green). These

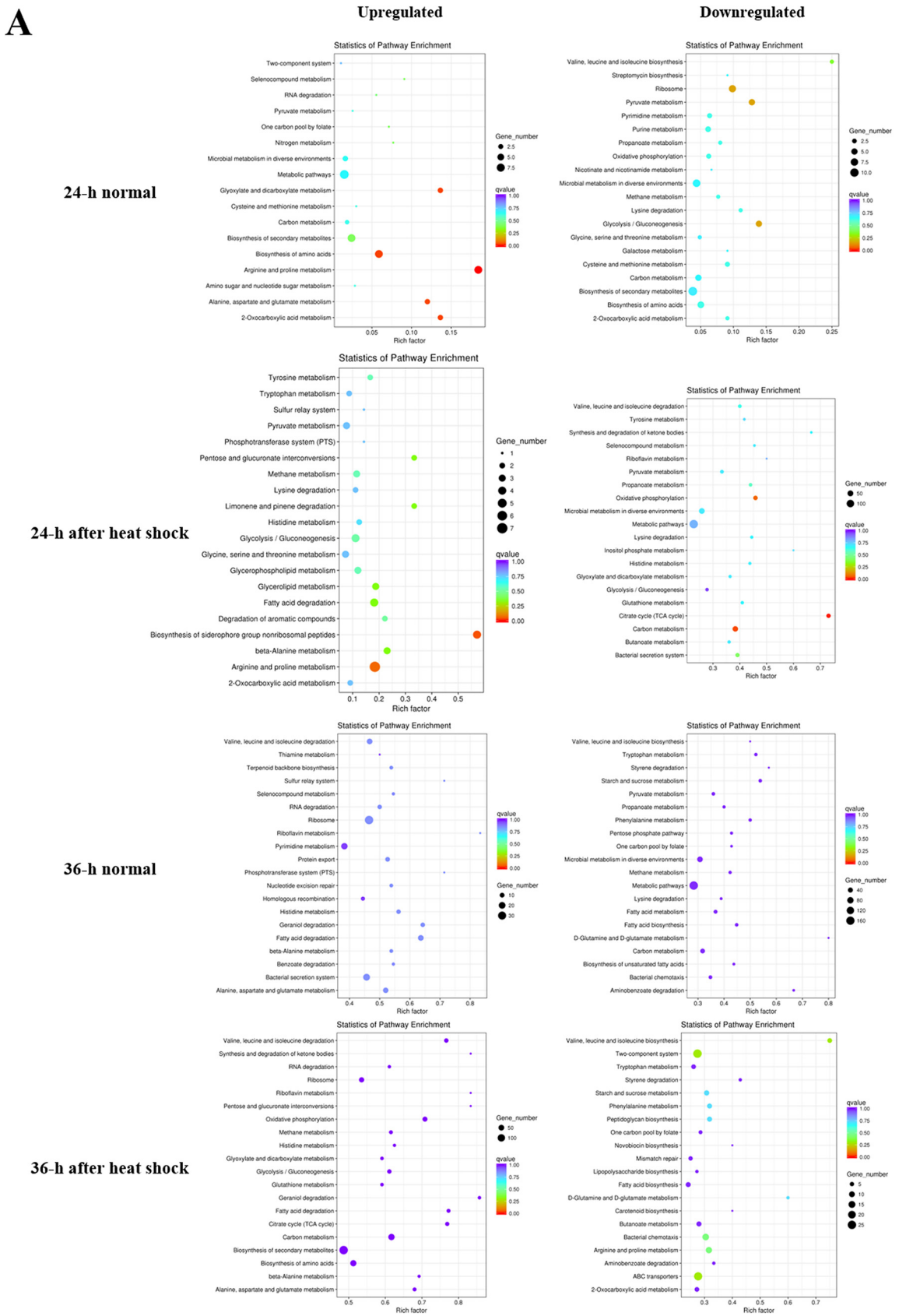


**FIG 4** Transcriptomic analysis of the *MXAN_4468* knockout mutants and the wild-type strain DK1622. (A) KEGG enrichment analysis of differentially expressed genes under different conditions. (B) Network analysis of the top 200 differentially expressed genes with high expression in all transcriptomic samples.

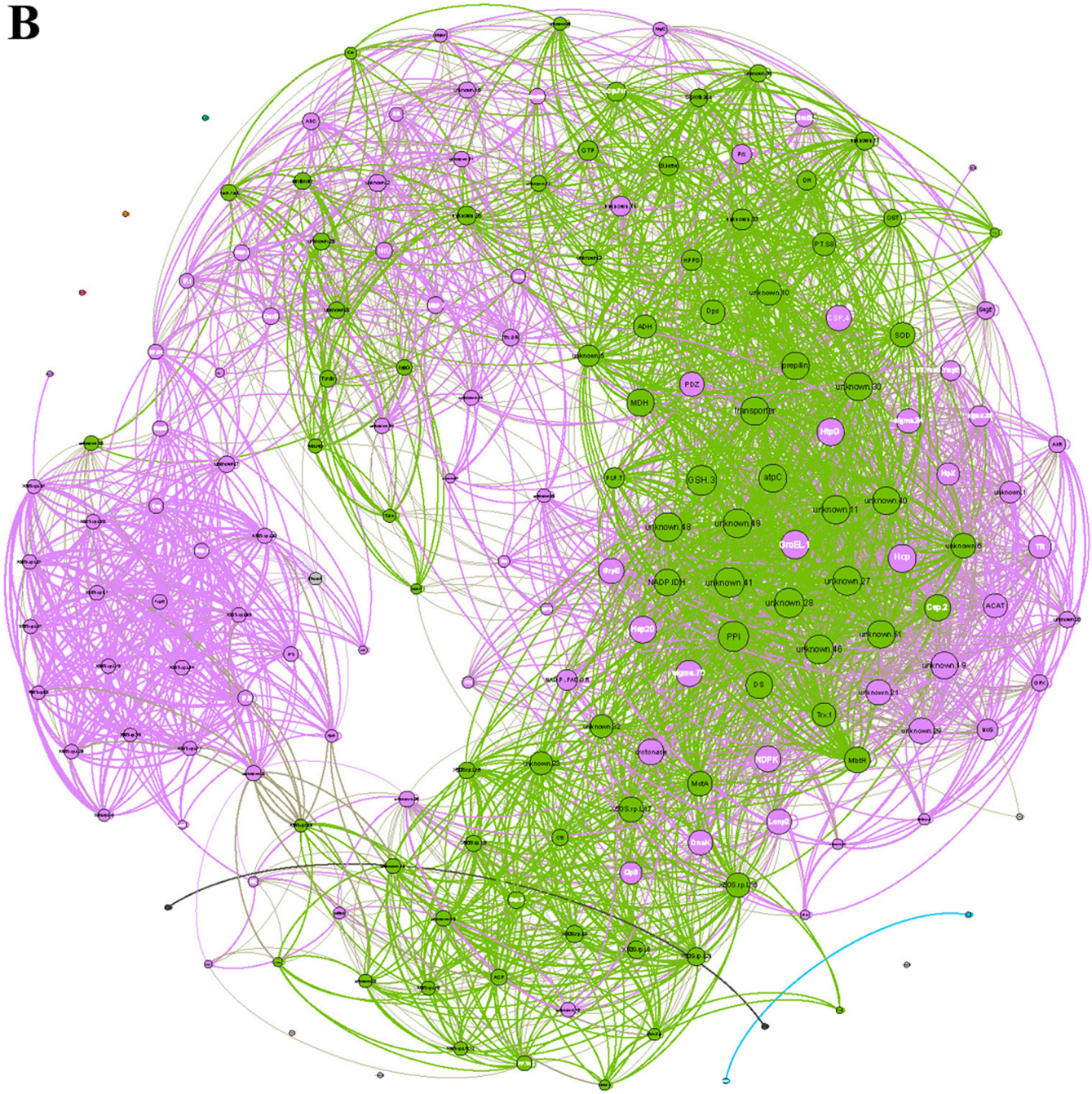


**FIG 4** Continued

results suggest that the transcription of the genes encoding stress regulatory proteins was regulated in a similar manner by *MXAN_4468* deletion; i.e., the orphan RR probably played a global negative regulatory role in the transcription of these genes.

***MXAN_4468* deletion decreases cell competition ability in *M. xanthus*.** *M. xanthus* cells have complex social behavior (30) and the ability to produce diverse secondary metabolites (31). We previously determined that the two *groEL* genes have divergent roles in development, predation, and biosynthesis of secondary metabolites (12–14). To efficiently achieve their cellular functions, the expression level of *groEL1* is about four times higher than that of *groEL2*, and their total expression level is approximately equal to the expression level of *groES*, the cochaperone gene of the duplicate *groEL*s (11). However,

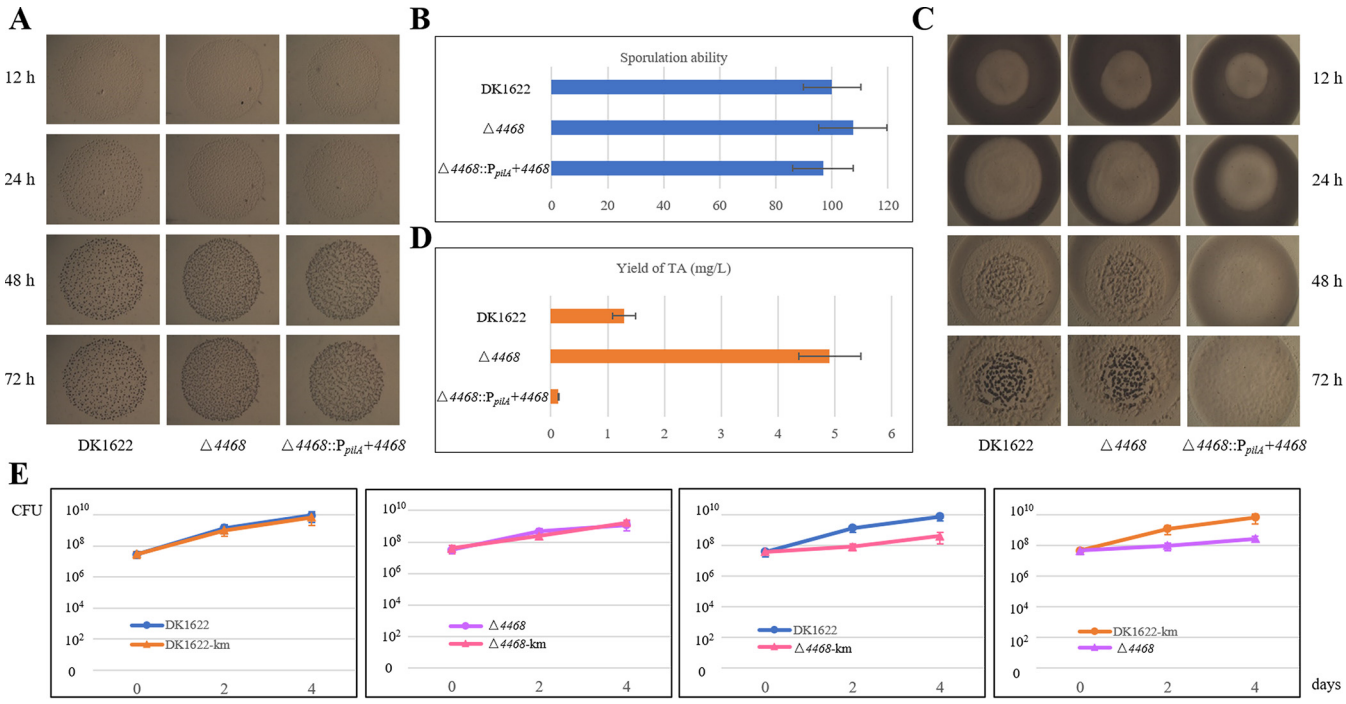


**FIG 5** Growth competition and social behavior analyses of the *MXAN_4468* mutants and the wild-type strain DK1622. The development (A), sporulation ability (B), predation (C), and myxovirescin (TA) fermentation level (D) analysis of the *MXAN_4468* knockout and overexpression mutants and the wild-type strain DK1622 are shown. The sporulation ability of DK1622 was set to 100. (E) Coincubation assays of the kanamycin-resistant strain DK1622-km (Δ*4468*-km) and the kanamycin-sensitive strain DK1622 (Δ*4468*). The strains were mixed in a 1:1 ratio and cocultured for 0, 2, and 4 days.

deletion of the *MXAN_4468* gene led to not only high expressions of the duplicate *groEL* genes but also unbalanced transcription of *groES* and *groEL*s. We found that the *MXAN_4468* deletion had almost no effects on development, sporulation, and predation abilities of *M. xanthus* (Fig. 5A to C) but markedly increased the biosynthesis of myxovirescin (Fig. 5D). In contrast, the *in situ* overexpression of *MXAN_4468*, which had almost no effect on the transcription of *groES* and *groEL1* but significantly decreased the transcription of *groEL2* (Fig. 1D), had no effects on development and sporulation but caused a weak deficiency in predation and led to near-undetectable myxovirescin biosynthesis. Thus, overexpression of *groEL1* or *groEL2* allowed or improved their related cellular functions but caused no effect on their unrelated functions; i.e., *groEL1* plays an essential role in fruiting body development and sporulation, while *groEL2* is required in predation and myxovirescin biosynthesis (12–14).

Although the high and unbalanced transcription of *groES* and *groEL*s had no significant effects on social behavior, it should be a metabolic burden to the host (32–34) and probably led to weaker competitive ability than that exhibited by the wild-type strain. To assay their growth competitive abilities, we constructed kanamycin-resistant strains of *M. xanthus* DK1622 and the Δ*4468* mutant and cocultured wild-type and mutant strains to form a competitive environment following the previous protocol (35). When the kanamycin-resistant and -sensitive DK1622 or Δ*4468* strains were cocultured on a casitone-based rich-nutrient (CTT) plate for 0, 2, and 4 days, the two types of cells in the harvested mixtures had the same number of CFU. However, when kanamycin-resistant Δ*4468* and -sensitive DK1622, or kanamycin-resistant DK1622 and -sensitive Δ*4468*, were mixed for cocultivation, the growth of the Δ*4468* mutant was significantly slower than that of the wild-type DK1622 (Fig. 5E). These results indicate that *MXAN_4468* deletion weakened the competitive ability of cells, probably due to the metabolic burden of high and unbalanced transcription of *groES* and *groEL*s.

## DISCUSSION

There are multiple copies in the DK1622 genome of the genes that encode single-domain RR proteins (Table S1). Seven of them are located in different chemosensory

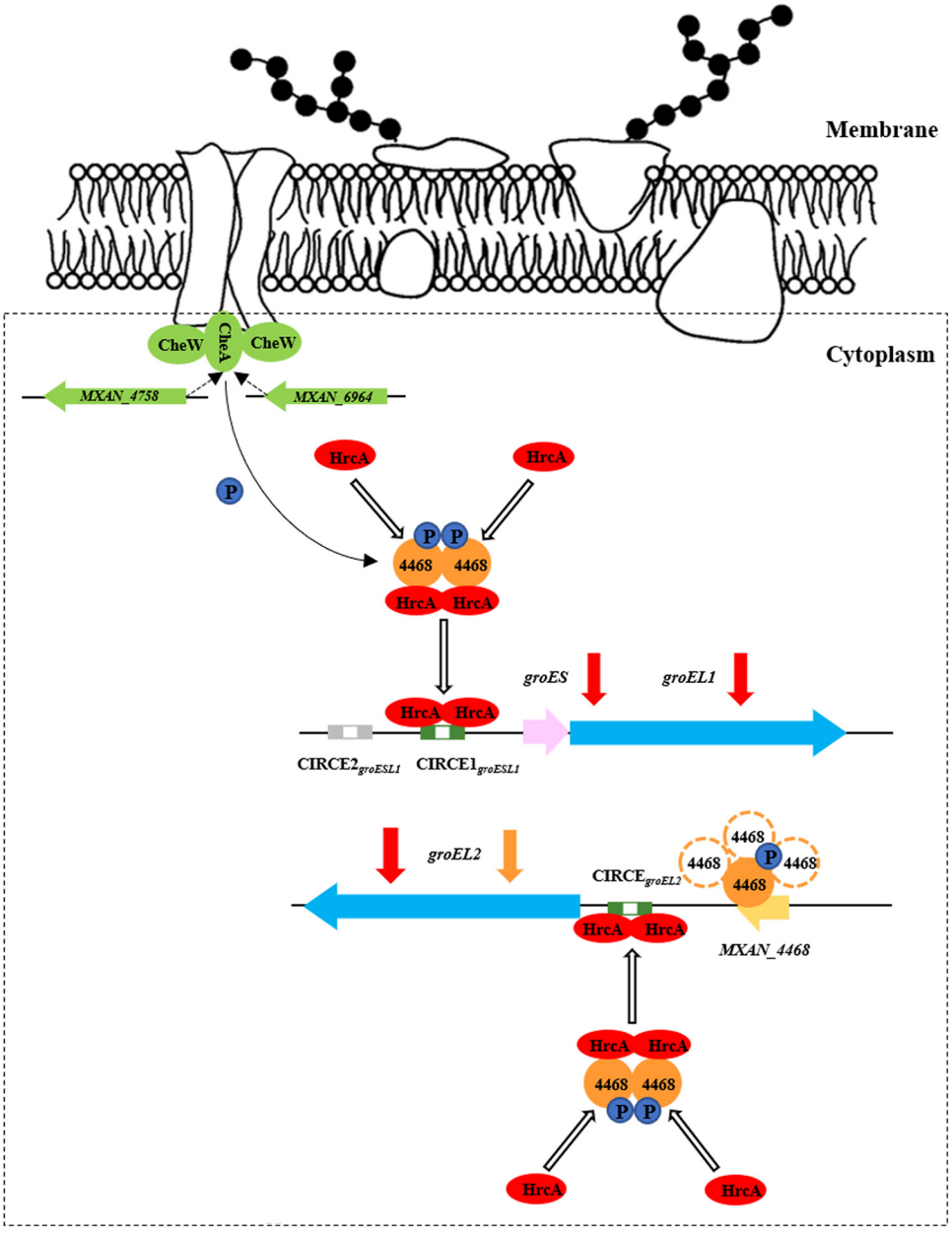


**FIG 6** Schematic of the transcriptional regulation of *groES* and *groELs* by MXAN_4468 in *M. xanthus* DK1622.

pathways (21) and the rest are orphan ones, like *MXAN_4468*. Previous studies have revealed that *MXAN_6693* (*difD*) in the Dif system (the Che2 system) is related to the chemotaxis of lipids (36, 37), *MXAN_2684* and *MXAN_6956*, belonging to the Che4 and Che6 systems, respectively, are both responsible for aggregation and sporulation (38, 39), and *MXAN_6965* in the Che7 system is important for resistance to temperature stress and for the production of viable spores (26). Little is known as yet about the function of the Che8 chemosensory pathway, as well as the substantial orphan RRs. In this study, we found that an orphan RR (MXAN_4468) plays a central role in tuning the transcriptional differences of *groESLs* via a novel functioning mode. First, the RR binds to HrcA and thereby enhances its ability to bind to the CIRCE elements, which enables it to achieve the transcriptional inhibition of the duplicate *groELs*. Second, the RR binds to the 3′ end of its own gene sequence, thereby specifically decreasing the transcription of the following *groEL2* gene. These functions require phosphorylation of the 61$^{st}$

aspartic acid residue of the RR. In addition to these specific functions, MXAN_4468 is probably involved in global regulation of cellular functions, indicated by significant transcriptomic changes caused by *MXAN_4468* deletion. The genes specifically regulated by MXAN_4468 are the duplicate *groEL*s, whose encoded proteins play essential roles in protein folding, assembly, and transport. In addition, pull-down results showed that MXAN_4468 could bind to some other transcriptional regulators and kinases (Table S2). It is thus unclear whether the transcriptomic changes were caused by MXAN_4468 directly, by GroELs indirectly, or by both.

In *Bacillus subtilis* cells, the HrcA protein is usually present in an inactive monomer form (40, 41), which is dimerized into an active form for binding to the CIRCE elements (42). Structural modeling indicated that dimerized MXAN_4468 is much more stable than dimerized HrcA (the dimerization energy of HrcA is −1.32, but that of the MXAN_4468 dimer is −95.77 [Fig. S5A]; the binding energy between MXAN_4468 and HrcA is −26.73 [Fig. S5B]). We posit that the MXAN_4468 dimer may recruit and bind to HrcA, consequently improving the formation of an active HrcA dimer for binding to the CIRCE elements in the promoter region of the duplicate *groEL*s. We propose a functioning model for the negative regulatory role of MXAN_4468 in the transcription of *groEL*s in *M. xanthus* cells (Fig. 6). The regulation of *groESL1* by MXAN_4468 via the recruitment of HrcA leads to the formation of a more active dimer to play a negative regulatory role in combination with CIRCE. This protein-protein interaction may promote the binding of this negative regulator to its target sequence, thus further enhancing its regulatory effect. In addition, to regulate *groEL2*, MXAN_4468, in polymeric forms, bound to the internal sequence of its own gene to further inhibit the transcription of *groEL2*. The binding of the MXAN_4468 protein to the *MXAN_4468* 3′-end DNA sequence was analyzed using nucleic acid-protein dock (NPdock) software (43), which showed that the C-terminal region of MXAN_4468 was likely responsible for binding to its own gene sequence on a 12-bp reverse complementary palindromic sequence (Fig. S5C).

There are 119 RRs in *M. xanthus*, and more than 50% of them are orphan. MXAN_4468 is a typical orphan RR; i.e., its function requires phosphorylation but without an HK gene adjacent on the genome (8). Here, we report that two noncognate HKs are the upstream components of MXAN_4468. The two corresponding *cheA* genes, i.e., *MXAN_6964* and *MXAN_4758*, belong to the Che7 and Che8 systems, respectively (21). Many organisms carry a substantial fraction of their two-component genes as orphans probably from duplication or loss of one component, which might be a mechanism for generating cross-regulation systems (44). The cross talk between noncognate HKs and an orphan RR (45) suggests complex and global regulation of MXAN_4468. Our network analysis suggested that among the multiple RR copies in *M. xanthus* DK1622, the special location of *MXAN_4468* may have extensive effects on the expression of stress regulatory proteins and yet have no correlation with other RR genes involved in the regulation of transcription. The global transcriptional effects of MXAN_4468 may be directly or indirectly related to the functions of *groEL*s. We speculate that in bacteria possessing multiple copies of orphan RR genes, these RR genes are involved in regulating the transcriptional symphony in cells to ensure that complex biological functions can occur.

## MATERIALS AND METHODS

**Cultures, plasmids, and growth conditions.** The strains, plasmids, and primers that were used in this study are shown in Table S4. The *M. xanthus* strains were cultivated in CTT medium (46) for growth assays. *E. coli* strains were routinely grown on LB agar or in LB broth. *E. coli* strains were grown at 37°C, while *Myxococcus* strains were incubated at 30°C. The temperature for heat shock treatment was 42°C. When required, kanamycin, ampicillin, and chloramphenicol were added to the media at final concentrations of 40, 100, and 34 $\mu$g/mL, respectively.

**Evolutionary relationship analysis.** The analysis of evolutionary relationships was completed using MEGA6 software (47). Briefly, protein sequences were constructed by the neighbor-joining method (NJ model) and pairwise deleted (pairwise deletion of gaps), and different evolutionary tree models were selected according to the type of protein. All tree self-expansion tests were set at 1,000 repeats to evaluate the stability of the nodes.

**Deletion of *MXAN_4758*, *MXAN_6964*, *MXAN_6692*, *MXAN_4468*, or *MXAN_4468* and *hrcA*.** An in-frame deletion in *M. xanthus* was performed using the positive-negative KG cassettes described by Ueki et al. (48). Genomic DNA from DK1622 served as the template for the PCR amplification of the upstream and downstream homologous arms using Phanta Super-Fidelity DNA polymerase (Vazyme). The fragments were cloned into SmaI-digested pBJ113 to construct the deletion plasmid pBJ-*4758*, pBJ-*6964*, pBJ-*6692*, or pBJ-*4468*, which was then transferred via electroporation into *M. xanthus* DK1622 cells. Individual kanamycin-resistant colonies were selected and then inoculated onto CTT agar plates supplemented with 1% galactose for the second round of screening. Deletion mutants were identified by the phenotypes of galactose resistance and kanamycin sensitivity, as well as by PCR verification. The *MXAN_4468* and *hrcA* double-knockout mutant was based on the *MXAN_4468* knockout mutant, in which the *hrcA* gene was deleted.

**Construction of *MXAN_4468 in situ* complement or overexpression mutant.** An *MXAN_4468 in situ* complement or overexpression mutant was constructed on the basis of the obtained *MXAN_4468* knockout mutant, and then a *4468* or $P_{pilA}$ plus *4468* fragment was inserted *in situ* by the secondary homologous recombination method to construct the *in situ* complement or overexpression mutant.

**qPCR analysis.** *M. xanthus* DK1622 and mutants were inoculated into CTT medium at an initial concentration of $1 \times 10^7$ cells/mL and collected after 24 h of incubation. The cultures were harvested at the testing time points, and the RNA was extracted immediately using a bacterial total RNA isolation kit (Sangon Biotech) according to the manufacturer's instructions. The purified RNA extracts were reverse transcribed to cDNA. Quantitative real-time PCR was performed with a total reaction volume of 20 $\mu$L containing 1 $\mu$L of 250 nM primers, 10 $\mu$L of SYBR green PCR master mix, 8.5 $\mu$L of RNase-free water, and 0.5 $\mu$L of a 10-fold-diluted cDNA template. The *gapA* gene was used as the reference. The primers for real-time PCR are listed in Table S4.

**Transcriptome analysis.** Differential expression analysis of *M. xanthus* DK1622 and mutants subjected to two temperature conditions (normal and heat shock) was performed using the DESeq R package (1.18.0) (49). DESeq provides statistical routines for determining differential expression in digital gene expression data using a model based on the negative binomial distribution. The resulting *P* values were adjusted using Benjamini and Hochberg's approach (50) for controlling the false-discovery rate. Genes found by DESeq and with an adjusted *P* value of less than 0.05 were assigned as differentially expressed.

The Kyoto Encyclopedia of Genes and Genomes (KEGG) is a database resource for understanding high-level functions and utilities of a biological system, such as a cell, an organism, and an ecosystem, from molecular-level information, especially large-scale molecular data sets generated by genome sequencing and other high-throughput experimental technologies (http://www.genome.jp/kegg/) (51). We used KEGG Orthology-Based Annotation System software to test the statistical enrichment of differentially expressed genes in KEGG pathways.

**Network analysis.** The network was based on the transcriptomic data, such that each node (or vertex) in the network represents a gene (or a protein), and each edge indicates a strong and significant transcriptional correlation. All analyses were performed in R version 3.5.0. The degree of centrality of each node was measured to determine the importance of nodes in the network. Accordingly, all of the nodes were classified into three categories based on the abundance of links with other members in the network: key nodes (vertices with the top 20% centrality), peripheral nodes (vertices with the lowest 20% centrality), and moderate nodes (the remainder of the vertices). All analyses were performed using psych package version 1.8.4 (52).

**Protein structure modeling analysis.** Based on the amino acid sequence of the individual wild-type and mutant protein, the protein structures were modeled using the I-TASSER tool (https://zhanglab.ccmb.med.umich.edu/I-TASSER/) (53). Prediction of protein-protein interactions was performed using the Prism 2.0 tool (http://cosbi.ku.edu.tr/prism/) (54).

**Cell phenotypic analysis. (i) Analysis of developmental ability and calculation of sporulation rate.** Briefly, each strain was cultured in CTT/CTT-resistant liquid medium for 20 to 24 h, and then the bacterial concentrations of the growing cultures were adjusted to $5 \times 10^9$ cells/mL (optical density at 600 nm [$OD_{600}$] = 35). Subsequently, 10-$\mu$L volumes of bacterial solutions were added onto TPM (Tris-HCl phosphate medium) plates, and the plates were incubated at 30°C. The development of fruiting bodies was observed and recorded using a stereoscopic microscope at 12-h intervals. After 5 days of culture, five fruiting bodies of each strain were scraped and cultured in the same centrifugal tube, 100 $\mu$L of TPM buffer was added to the tubes, and the bacterial suspensions were subjected to three treatments of low-power ultrasound (<200 W, 4 s) to evenly disperse the cells. The suspensions were then incubated in a bath at 50°C for 2 h. The treated spore suspensions were diluted 10 times with TPM buffer. Subsequently, 50-$\mu$L bacterial suspensions of appropriate dilutions were mixed evenly with melted CTT soft agar (0.3% agar) and spread onto CTT/CTT-resistant plates. This process was repeated three times for every strain suspension. The plates were cultured at 30°C for 5 days, and then the number of colonies on the plates was counted and the sporulation rate of each strain was calculated.

**(ii) Analysis of predation ability.** *E. coli* DH5$\alpha$ was cultured in LB liquid medium for 12 h. Based on the detected $OD_{600}$ value, the bacterial concentration was adjusted to an $OD_{600}$ of 100 using TPM buffer, and 30 $\mu$L was inoculated onto a water (WAT) plate (containing only $CaCl_2$). The mutants and wild-type strain of *Myxococcus* were cultured in CTT liquid medium for 20 to 24 h. The bacterial concentrations of these growing bacterial cultures were adjusted to $5 \times 10^9$ cells/mL ($OD_{600}$ = 35) using TPM buffer, and 2 $\mu$L of each bacterial suspension was inoculated onto the middle of an *E. coli*-inoculated WAT plate. This process was repeated three times for every strain suspension. After drying, the colonies were

incubated at 30°C. The predation activity was observed and photographed using a stereoscopic microscope at 12-h intervals.

**Determination of the fermentation level of myxovirescin (TA).** The wild-type DK1622 and mutants were activated on CTT/CTT-resistant solid plates and inoculated into CYE liquid medium for 20 to 24 h. Subsequently, 1% ion-exchange resin was added to each medium, and the culturing was continued for approximately 2 days until the later stage of growth stability. The supernatant was removed to collect the bacteria and resin, and the bacteria were gently washed with double-distilled water ($ddH_2O$). Each sample was extracted with approximately 8 mL of methanol and shaken overnight at a uniform speed. This step was repeated two more times. The combined extracts were concentrated to approximately 3 mL using a vacuum concentration dryer. The concentrated solution was centrifuged at 12,000 rpm for 15 min at 4°C, and the supernatant was used for the next step. The production of TA in each strain was detected by HPLC with a *Myxococcus* (TA) standard as a control.

**MXAN_4468 protein purification.** The heterogeneously expressed MXAN_4468 proteins were purified with some modifications. BL21 cells were grown at 37°C in LB medium with 100 $\mu$g/mL of ampicillin to an $OD_{600}$ of 0.6 to 0.8 and were induced with 1 mM isopropyl-$\beta$-D-thiogalactopyranoside (IPTG). The cells were resuspended in lysis buffer (25 mM Tris-HCl [pH 8.0], 300 mM NaCl, 2 mM dithiothreitol) and sonicated. After gentle ultrasonic treatment, the samples were centrifuged at 12,000 rpm for 30 min at 4°C. The supernatant of His-tagged MXAN_4468 was applied on $Ni^{2+}$-nitrilotriacetic acid (NTA) and then purified by ion-exchange chromatography using a Sephadex 200 gel filtration column. The protein concentration was determined using a microconcentration detector.

**EMSAs.** The purified MXAN_4468 proteins with different concentrations were incubated with DNA at 30°C for 30 min and then subjected to nondenatured polypropylene gel electrophoresis (90 V, 1 h). The gel was visualized by detecting chemiluminescence after blocking it with the solution and antibody (streptavidin-horseradish peroxidase [HRP]) in the electrophoretic mobility shift assay (EMSA) kit (Thermo Fisher).

**Construction of key site mutation expression vector and mutant strains.** The aspartic acid at position 61 (GAC) of MXAN_4468 was mutated to valine (GTC) or phenylalanine (TTC). The expression vectors pET32a, with a His tag, and pMAL-c5X, with an MBP tag, were selected. The mutation-harboring recombinant vector was constructed using the ClonExpress II one-step cloning kit (Vazyme). The same homologous recombination method was used to construct a pBJ113 plasmid containing the *MXAN_4468* gene with a key site mutation, together with its upstream and downstream homologous arms.

**Phos-tag PAGE.** A His tag was attached to the C terminus of MXAN_4468 and the mutant proteins. To ensure correct formation of the spatial structure of the fusion protein, a linker sequence (TCTG GCTCGAGCTCTGGCGCGCCGGGC) was added between the fusion parts. Phos-tag composite electrophoresis adhesive was prepared using the Phos-tag acrylamide AAL-107 kit. When electrophoresis was performed in the Phos-tag composite electrophoresis gel, the specific binding of Phos-tag to the phosphate group of the phosphorylated protein hindered its migration, resulting in lower mobility of the phosphorylated protein than of the unphosphorylated protein (55). During the experiment, a sufficient amount of commercialized histidine protein kinase (L-histidine K1) was added to activate the phosphorylation of MXAN_4468.

**Pull-down analysis for potential binding proteins.** The mixtures of 4468-pMAL, 4468-D61V-pMAL, and 4468-D61F-pMAL were induced and purified, and pMAL (MBP-tagged protein) was established as the negative control. Strain DK1622 cultured on solid medium was transferred to CTT liquid medium and cultured for 20 to 24 h. The cells were collected by centrifugation, washed three times with TPM buffer, then suspended in a heavy suspension buffer, and lysed by ultrasound. After centrifugation, appropriate amounts of supernatant and 4468-MBP plus MBP filler, 4468-D61V-MBP plus filler, 4468-D61F-MBP plus filler, MBP plus filler, or only filler were mixed and incubated at 4°C for 4 h. The incubated mixture was washed through the column with buffer, and then 10 mM maltose was added to elute MXAN_4468 and the protein bound to the filler. The eluted-protein-containing solutions obtained from the experimental and control groups were sent to Shanghai Zhong Ke Xin Sheng Ming Company for identification by mass spectrometry.

**Co-culture of strains.** The nonresistant and resistant strains were cultured in CTT/CTT-km liquid medium at 30°C for 20 to 24 h. The cells were collected, and their concentrations were adjusted to $5 \times 10^9$ cells/mL. The nonresistant and resistant strains were mixed at a 1:1 (vol/vol) ratio, and 5-$\mu$L volumes of the obtained bacterial solutions were inoculated onto CTT plates. After culturing at 30°C for 0, 2, and 4 days, the whole colonies were scraped and resuspended in 500 $\mu$L of TPM buffer. The resulting bacterial suspensions were diluted 10 times, and the suitable four dilutions of three repeated 50-$\mu$L suspensions were mixed evenly with 2.5 mL of semisolid CTT (0.3% agar) and then spread onto the CTT/CTT-km plates. After 5 days of culture, the number of colonies on the plate was counted and the CFU of each strain were calculated.

## SUPPLEMENTAL MATERIAL

Supplemental material is available online only.

**DATA SET S1**, XLSX file, 0.5 MB.

**FIG S1**, TIF file, 1.6 MB.

**FIG S2**, TIF file, 2.9 MB.

**FIG S3**, TIF file, 2.2 MB.

**FIG S4**, TIF file, 0.7 MB.

**FIG S5**, TIF file, 2.6 MB.
**TABLE S1**, DOCX file, 0.03 MB.
**TABLE S2**, DOCX file, 0.04 MB.
**TABLE S3**, DOCX file, 0.03 MB.
**TABLE S4**, DOCX file, 0.03 MB.

## ACKNOWLEDGMENTS

We thank Zheng Zhang for his helpful discussion and Zhifeng Li, Jing Zhu, Jingyao Qu, and Guannan Lin from the State Key Laboratory of Microbial Technology of Shandong University for help and guidance with the quantitative fluorescence PCR instrument.

This work was financially supported by funds from the National Key Research and Development Program (2018YFA0900400 and 2018YFA0901704), the National Natural Science Foundation of China (31670076), the Special Investigation on Scientific and Technological Basic Resources (2017FY100300), and the Key Research and Development Program of Shandong Province (2018GSF121015) awarded to Yue-zhong Li. This work was also supported by funds from the National Postdoctoral Program for Innovative Talents of China (BX20190190) and Qingdao Postdoctoral Application Research Project of China (62450070311096) awarded to Li Zhuo.

## REFERENCES

1. Stock AM, Robinson VL, Goudreau PN. 2000. Two-component signal transduction. Annu Rev Biochem 69:183–215. https://doi.org/10.1146/annurev.biochem.69.1.183.
2. West AH, Stock AM. 2001. Histidine kinases and response regulator proteins in two-component signaling systems. Trends Biochem Sci 26:369–376. https://doi.org/10.1016/s0968-0004(01)01852-7.
3. Groisman EA. 2016. Feedback control of two-component regulatory systems. Annu Rev Microbiol 70:103–124. https://doi.org/10.1146/annurev-micro-102215-095331.
4. Mizuno T. 1997. Compilation of all genes encoding two-component phosphotransfer signal transducers in the genome of *Escherichia coli*. DNA Res 4:161–168. https://doi.org/10.1093/dnares/4.2.161.
5. Song LF, Sudhakar P, Wang W, Conrads G, Brock A, Sun JB, Wagner-Dobler I, Zeng AP. 2012. A genome-wide study of two-component signal transduction systems in eight newly sequenced mutans streptococci strains. BMC Genomics 13:128. https://doi.org/10.1186/1471-2164-13-128.
6. Casella LG, Weiss A, Perez-Rueda E, Ibarra JA, Shaw LN. 2017. Towards the complete proteinaceous regulome of *Acinetobacter baumannii*. Microb Genom 3:mgen000107. https://doi.org/10.1099/mgen.0.000107.
7. Shi XQ, Wegener-Feldbrugge S, Huntley S, Hamann N, Hedderich R, Sogaard-Andersen L. 2008. Bioinformatics and experimental analysis of proteins of two-component systems in *Myxococcus xanthus*. J Bacteriol 190:613–624. https://doi.org/10.1128/JB.01502-07.
8. McLean TC, Lo R, Tschowri N, Hoskisson PA, Al Bassam MM, Hutchings MI, Som NF. 2019. Sensing and responding to diverse extracellular signals: an updated analysis of the sensor kinases and response regulators of *Streptomyces* species. Microbiology (Reading) 165:929–952. https://doi.org/10.1099/mic.0.000817.
9. Houry WA, Frishman D, Eckerskorn C, Lottspeich F, Hartl FU. 1999. Identification of *in vivo* substrates of the chaperonin GroEL. Nature 402:147–154. https://doi.org/10.1038/45977.
10. Kerner MJ, Naylor DJ, Ishihama Y, Maier T, Chang HC, Stines AP, Georgopoulos C, Frishman D, Hayer-Hartl M, Mann M, Hartl FU. 2005. Proteome-wide analysis of chaperonin-dependent protein folding in *Escherichia coli*. Cell 122:209–220. https://doi.org/10.1016/j.cell.2005.05.028.
11. Zhuo L, Wang Y, Zhang Z, Li J, Zhang XH, Li YZ. 2017. *Myxococcus xanthus* DK1622 coordinates expressions of the duplicate *groEL* and single *groES* genes for synergistic functions of GroELs and GroES. Front Microbiol 8:733. https://doi.org/10.3389/fmicb.2017.00733.
12. Li J, Wang Y, Zhang CY, Zhang WY, Jiang DM, Wu ZH, Liu H, Li YZ. 2010. *Myxococcus xanthus* viability depends on *groEL* supplied by either of two genes, but the paralogs have different functions during heat shock, predation, and development. J Bacteriol 192:1875–1881. https://doi.org/10.1128/JB.01458-09.
13. Wang Y, Zhang WY, Zhang Z, Li J, Li ZF, Tan ZG, Zhang TT, Wu ZH, Liu H, Li YZ. 2013. Mechanisms involved in the functional divergence of duplicated GroEL chaperonins in *Myxococcus xanthus* DK1622. PLoS Genet 9:e1003306. https://doi.org/10.1371/journal.pgen.1003306.
14. Wang Y, Li X, Zhang W, Zhou X, Li YZ. 2014. The *groEL2* gene, but not *groEL1*, is required for biosynthesis of the secondary metabolite myxovirescin in *Myxococcus xanthus* DK1622. Microbiology (Reading) 160:488–495. https://doi.org/10.1099/mic.0.065862-0.
15. Zhuo L, Zhang Z, Pan Z, Sheng D-H, Hu W, Li Y-Z. 2018. CIRCE element evolved for the coordinated transcriptional regulation of bacterial duplicate *groELs*. Biochim Biophys Acta Gene Regul Mech 1861:928–937. https://doi.org/10.1016/j.bbagrm.2018.08.003.
16. Zschiedrich CP, Keidel V, Szurmant H. 2016. Molecular mechanisms of two-component signal transduction. J Mol Biol 428:3752–3775. https://doi.org/10.1016/j.jmb.2016.08.003.
17. Bellsolell L, Prieto J, Serrano L, Coll M. 1994. Magnesium binding to the bacterial chemotaxis protein CheY results in large conformational changes involving its functional surface. J Mol Biol 238:489–495. https://doi.org/10.1006/jmbi.1994.1308.
18. Banerjee R, Das S, Mukhopadhyay K, Nag S, Chakrabortty A, Chaudhuri K. 2002. Involvement of *in vivo* induced cheY-4 gene of *Vibrio cholerae* in motility, early adherence to intestinal epithelial cells and regulation of virulence factors. FEBS Lett 532:221–226. https://doi.org/10.1016/s0014-5793(02)03678-5.
19. Burbulys D, Trach KA, Hoch JA. 1991. Initiation of sporulation in *B. subtilis* is controlled by a multicomponent phosphorelay. Cell 64:545–552. https://doi.org/10.1016/0092-8674(91)90238-T.
20. Inclan YF, Vlamakis HC, Zusman DR. 2007. FrzZ, a dual CheY-like response regulator, functions as an output for the Frz chemosensory pathway of *Myxococcus xanthus*. Mol Microbiol 65:90–102. https://doi.org/10.1111/j.1365-2958.2007.05774.x.
21. Zusman DR, Scott AE, Yang Z, Kirby JR. 2007. Chemosensory pathways, motility and development in *Myxococcus xanthus*. Nat Rev Microbiol 5:862–872. https://doi.org/10.1038/nrmicro1770.
22. Kothe M, Kohls D, Low S, Coli R, Cheng AC, Jacques SL, Johnson TL, Lewis C, Loh C, Nonomiya J, Sheils AL, Verdries KA, Wynn TA, Kuhn C, Ding YH. 2007. Structure of the catalytic domain of human polo-like kinase 1. Biochemistry 46:5960–5971. https://doi.org/10.1021/bi602474j.
23. Kumar S, Sarkar P, Sim MJ, Rajagopalan S, Vogel SS, Long EO. 2015. A single amino acid change in inhibitory killer cell Ig-like receptor results in constitutive receptor self-association and phosphorylation. J Immunol 194:817–826. https://doi.org/10.4049/jimmunol.1401830.
24. Bhaya D, Takahashi A, Grossman AR. 2001. Light regulation of type IV pilus-dependent motility by chemosensor-like elements in *Synechocystis*

PCC6803. Proc Natl Acad Sci U S A 98:7540–7545. https://doi.org/10.1073/pnas.131201098.
25. Parkinson JS, Hazelbauer GL, Falke JJ. 2015. Signaling and sensory adaptation in *Escherichia coli* chemoreceptors: 2015 update. Trends Microbiol 23:257–266. https://doi.org/10.1016/j.tim.2015.03.003.
26. Darnell CL, Wilson JM, Tiwari N, Fuentes EJ, Kirby JR. 2014. Chemosensory regulation of a HEAT-repeat protein couples aggregation and sporulation in *Myxococcus xanthus*. J Bacteriol 196:3160–3168. https://doi.org/10.1128/JB.01866-14.
27. Lund PA. 2001. Microbial molecular chaperones. Adv Microb Physiol 44:93–140. https://doi.org/10.1016/s0065-2911(01)44012-4.
28. Lund PA. 2009. Multiple chaperonins in bacteria—why so many? FEMS Microbiol Rev 33:785–800. https://doi.org/10.1111/j.1574-6976.2009.00178.x.
29. Langmead B, Salzberg SL. 2012. Fast gapped-read alignment with Bowtie 2. Nat Methods 9:357–359. https://doi.org/10.1038/nmeth.1923.
30. Dworkin M. 1996. Recent advances in the social and developmental biology of the myxobacteria. Microbiol Rev 60:70–102. https://doi.org/10.1128/mr.60.1.70-102.1996.
31. Wenzel SC, Muller R. 2009. Myxobacteria—'microbial factories' for the production of bioactive secondary metabolites. Mol Biosyst 5:567–574. https://doi.org/10.1039/b901287g.
32. Birnbaum S, Bailey JE. 1991. Plasmid presence changes the relative levels of many host cell proteins and ribosome components in recombinant *Escherichia coli*. Biotechnol Bioeng 37:736–745. https://doi.org/10.1002/bit.260370808.
33. Rozkov A, Avignone-Rossa CA, Ertl PF, Jones P, O'Kennedy RD, Smith JJ, Dale JW, Bushell ME. 2004. Characterization of the metabolic burden on *Escherichia coli* DH1 cells imposed by the presence of a plasmid containing a gene therapy sequence. Biotechnol Bioeng 88:909–915. https://doi.org/10.1002/bit.20327.
34. Chen XJ, Zhang Z, Li YJ, Zhuo L, Sheng DH, Li YZ. 2020. Insights into the persistence and phenotypic effects of the endogenous and cryptic plasmid pMF1 in its host strain *Myxococcus fulvus* 124B02. FEMS Microbiol Ecol 96:fiaa001. https://doi.org/10.1093/femsec/fiaa001.
35. Gong Y, Zhang Z, Liu Y, Zhou XW, Anwar MN, Li ZS, Hu W, Li YZ. 2018. A nuclease-toxin and immunity system for kin discrimination in *Myxococcus xanthus*. Environ Microbiol 20:2552–2567. https://doi.org/10.1111/1462-2920.14282.
36. Jarrell KF, McBride MJ. 2008. The surprisingly diverse ways that prokaryotes move. Nat Rev Microbiol 6:466–476. https://doi.org/10.1038/nrmicro1900.
37. Yang Z, Geng Y, Xu D, Kaplan HB, Shi W. 1998. A new set of chemotaxis homologues is essential for *Myxococcus xanthus* social motility. Mol Microbiol 30:1123–1130. https://doi.org/10.1046/j.1365-2958.1998.01160.x.
38. Lee KS, Shimkets LJ. 1996. Suppression of a signaling defect during *Myxococcus xanthus* development. J Bacteriol 178:977–984. https://doi.org/10.1128/jb.178.4.977-984.1996.
39. Vlamakis HC, Kirby JR, Zusman DR. 2004. The Che4 pathway of *Myxococcus xanthus* regulates type IV pilus-mediated motility. Mol Microbiol 52:1799–1811. https://doi.org/10.1111/j.1365-2958.2004.04098.x.
40. Mogk A, Homuth G, Scholz C, Kim L, Schmid FX, Schumann W. 1997. The GroE chaperonin machine is a major modulator of the CIRCE heat shock regulon of *Bacillus subtilis*. EMBO J 16:4579–4590. https://doi.org/10.1093/emboj/16.15.4579.
41. Reischl S, Wiegert T, Schumann W. 2002. Isolation and analysis of mutant alleles of the *Bacillus subtilis* HrcA repressor with reduced dependency on GroE function. J Biol Chem 277:32659–32667. https://doi.org/10.1074/jbc.M201372200.
42. Schumann W. 2003. The *Bacillus subtilis* heat shock stimulon. Cell Stress Chaperones 8:207–217. https://doi.org/10.1379/1466-1268(2003)008%3C0207:TBSHSS%3E2.0.CO;2.
43. Tuszynska I, Magnus M, Jonak K, Dawson W, Bujnicki JM. 2015. NPDock: a web server for protein-nucleic acid docking. Nucleic Acids Res 43:W425–W430. https://doi.org/10.1093/nar/gkv493.
44. Capra EJ, Laub MT. 2012. Evolution of two-component signal transduction systems. Annu Rev Microbiol 66:325–347. https://doi.org/10.1146/annurev-micro-092611-150039.
45. Wang WH, Shu D, Chen L, Jiang WH, Lu YH. 2009. Cross-talk between an orphan response regulator and a noncognate histidine kinase in *Streptomyces coelicolor*. FEMS Microbiol Lett 294:150–156. https://doi.org/10.1111/j.1574-6968.2009.01563.x.
46. Hodgkin J, Kaiser D. 1977. Cell-to-cell stimulation of movement in nonmotile mutants of *Myxococcus*. Proc Natl Acad Sci U S A 74:2938–2942. https://doi.org/10.1073/pnas.74.7.2938.
47. Tamura K, Stecher G, Peterson D, Filipski A, Kumar S. 2013. MEGA6: Molecular Evolutionary Genetics Analysis version 6.0. Mol Biol Evol 30:2725–2729. https://doi.org/10.1093/molbev/mst197.
48. Ueki T, Inouye S, Inouye M. 1996. Positive-negative KG cassettes for construction of multi-gene deletions using a single drug marker. Gene 183:153–157. https://doi.org/10.1016/s0378-1119(96)00546-x.
49. Anders S, Huber W. 2010. Differential expression analysis for sequence count data. Genome Biol 11:R106. https://doi.org/10.1186/gb-2010-11-10-r106.
50. Benjamini Y, Hochberg Y. 1995. Controlling the false discovery rate: a practical and powerful approach to multiple hypothesis testing. J R Stat Soc B 57:289–300. https://doi.org/10.1111/j.2517-6161.1995.tb02031.x.
51. Kanehisa M, Araki M, Goto S, Hattori M, Hirakawa M, Itoh M, Katayama T, Kawashima S, Okuda S, Tokimatsu T, Yamanishi Y. 2008. KEGG for linking genomes to life and the environment. Nucleic Acids Res 36:D480–D484. https://doi.org/10.1093/nar/gkm882.
52. Xian WD, Salam N, Li MM, Zhou EM, Yin YR, Liu ZT, Ming YZ, Zhang XT, Wu G, Liu L, Xiao M, Jiang HC, Li WJ. 2020. Network-directed efficient isolation of previously uncultivated Chloroflexi and related bacteria in hot spring microbial mats. NPJ Biofilms Microbiomes 6:20. https://doi.org/10.1038/s41522-020-0131-4.
53. Zhang Y, Skolnick J. 2005. TM-align: a protein structure alignment algorithm based on the TM-score. Nucleic Acids Res 33:2302–2309. https://doi.org/10.1093/nar/gki524.
54. Baspinar A, Cukuroglu E, Nussinov R, Keskin O, Gursoy A. 2014. PRISM: a web server and repository for prediction of protein-protein interactions and modeling their 3D complexes. Nucleic Acids Res 42:W285–W289. https://doi.org/10.1093/nar/gku397.
55. Nemoto K, Ramadan A, Arimura GI, Imai K, Tomii K, Shinozaki K, Sawasaki T. 2017. Tyrosine phosphorylation of the GARU E3 ubiquitin ligase promotes gibberellin signalling by preventing GID1 degradation. Nat Commun 8:1004. https://doi.org/10.1038/s41467-017-01005-5.